Renewable Energy 215 (2023) 118954

Contents lists available at ScienceDirect

Renewable Energy

journal homepage: www.elsevier.com/locate/renene

Role of permeability coefficients in salinity gradient energy generation by PRO systems with spiral wound membrane modules

A. Ruiz-García [a,*], F. Tadeo [b], I. Nuez [a]

[a] Department of Electronic Engineering and Automation, University of Las Palmas de Gran Canaria, Campus Universitario de Tafira, E-35017 Las Palmas de Gran Canaria, Spain

[b] Institute of Sustainable Processes, University of Valladolid, Spain

ARTICLE INFO

Keywords:
Pressure retarded osmosis
Salinity gradient
Energy generation
Renewable energy
Optimization
Membranes

ABSTRACT

Processes that can transform a salinity gradient into electrical energy have gained attention in recent years. One such process, which uses semipermeable membranes to generate electrical energy through a turbine, is pressure retarded osmosis (PRO). As a potential renewable energy technology, this process could also be integrated in desalination plants to reduce the energy consumption. However, principally because of certain drawbacks concerning membrane and module characteristics, PRO technology has not yet been fully exploited at commercial scale. This study aims to assess the impact of membrane permeability coefficients on the energy generated by full-scale single-stage PRO systems. This allow an evaluation of the performance of PRO modules in series considering variation of the permeability coefficients that may be due to the impact of fouling. An evaluation was made of the HTI OsMem™ 2521 spiral wound membrane module considering a diameter of 8 inches (high up-scaled active area) and different permeability coefficient ranges. The results showed that a 50% water permeability coefficient decrease would produce an approximately 25% decrease in the amount of energy that could be generated, while a 50% increase in the solute permeability coefficient would have virtually no effect when considering optimal operating points. Variation of the water permeability coefficient had more impact on the potential amount of generated energy than variation of the solute permeability coefficient.

1. Introduction

The increasing use of renewable energy sources (RES) is mainly due to concerns about climate change and greenhouse gas (GHG) emissions produced by fossil fuel energy sources [1,2]. Research continues into several technologies that allow the use of RES to provide sustainable and efficient energy solutions. One of the main challenges of using RES such as wind or solar energy is their variability, which makes it difficult to predict and manage power generation [3]. In consequence, expensive storage systems and/or fossil fuel-based energy generation systems are commonly required to overcome the problems of intermittent energy production caused by variable RES (VRES) [4,5]. The use of steady RES (SRES) would help the integration of VRES and allow replacement of fossil fuel-based power systems [6]. In this regard, the generation of energy from salinity gradients is considered a promising SRES [7–9]. This could have the additional advantage of reducing the environmental impact of brine discharge due to its dilution for energy generation [10–12]. Technologies that are being actively studied for salinity gradient energy generation include capacitive mixing and mixing entropy battery, forward osmosis–electrokinetic systems, pressure retarded osmosis (PRO) and reverse electrodialysis [13–15]. These technologies can be combined with several wastewater treatment technologies (e.g., thermal, membrane-based, chemical or electrochemical) for the removal of pollutants from brine effluents [16,17]. One of the most studied technologies is PRO [18], which has higher efficiency and power density [19] than others. However, the principal problem of PRO is its viability at pilot or full scale [20]. Key factors in this respect include improvement of membrane module properties through modeling [21,22], simulating and optimizing the process when using full-scale modules [23–25], module configuration [26,27], the feed spacer geometry [27] and the effect of fouling on performance [28–30]. As for the membrane properties, the water and solute permeability coefficients (A and B) play an important role in the performance of PRO membrane modules. Numerous studies on improving PRO membrane properties in terms of their permeability coefficients have been carried out [7,31,32].

She et al. [33] evaluated the effect of three different feed spacers in a flat sheet membrane made of cellulose triacetate. The obtained water permeability coefficients (A) were 4.17×10^{-12}, 4×10^{-12} and

* Corresponding author.
E-mail addresses: alejandro.ruiz@ulpgc.es (A. Ruiz-García), fernando.tadeo@uva.es (F. Tadeo), ignacio.nuez@ulpgc.es (I. Nuez).

https://doi.org/10.1016/j.renene.2023.118954
Received 6 December 2022; Received in revised form 3 February 2023; Accepted 23 June 2023
Available online 30 June 2023

Nomenclature

Acronyms

DS	Draw solution
ECP	External concentration polarization
ERD	Energy recovery device
FS	Feed solution
HF	Hollow fiber
ICP	Internal concentration polarization
PV	Pressure vessel
RES	Renewable energy sources
RO	Reverse osmosis
SRES	Steady renewable energy sources
SWMM	Spiral wound membrane module
SWRO	Seawater reverse osmosis
TFC	Thin-film composite
TNC	Thin-film nanofiber composite
VRES	Variable renewable energy sources

Variables

$\dot{m}$	Mass flow ($kg\,s^{-1}$)
A	Water permeability coefficient ($m\,Pa^{-1}\,s^{-1}$)
A_0	Initial water permeability coefficient ($m\,Pa^{-1}\,s^{-1}$)
B	Solute permeability coefficient ($m\,s^{-1}$)
CF	Concentration factor
C	Concentration ($g\,L^{-1}$ or kg (solute) kg^{-1} (water))
DF	Dilution factor
D	Solute diffusivity ($m^2\,s^{-1}$)
d_h	Hydraulic diameter of feed channel (m)
FF	Fouling factor
H	Spacer height (m)
h	Specific enthalpy ($J\,kg^{-1}$)
J	Flux per unit area ($m^3\,m^{-2}\,s^{-1}$)
K	Solute resistivity ($s\,m^{-1}$)
k	Mass transfer coefficient
K_λ	Parameter applied to friction factor
L	Length of the SWMM (m)
n	Number of SWMMs in PRO system
PD	Power density ($W\,m^{-2}$)
P	Power (W)
p	Pressure (Pa)
P_{ew}	Wall Péclet number
Q	Flow ($m^3\,h^{-1}$ or $m^3\,s^{-1}$)
R	Flux recovery (%)
Sc	Schmidt number
Sh	Sherwood number
S_m	Membrane surface area (m^2)
TCF	Temperature correction factor
T	Temperature (°C or K)

Greek letters

$\Delta\pi$	Osmotic pressure difference (Pa)
Δp	Pressure drop (Pa)
η	Performance
γ	Lumped parameter
μ	Dynamic viscosity (Pa s)
ν	Velocity ($m\,s^{-1}$)
π	Osmotic pressure (Pa)
ρ	Density ($kg\,m^{-3}$)
ε	Porosity in feed channel
ϑ	specific volume $m^3\,kg^{-1}$

Subscripts

av	Average
D	Draw
F	Feed
id	Ideal
in	Input
m	Membrane
out	Output
p	Permeate
TB	Turbine
x	Draw or feed

2.78×10^{-12} $m\,Pa^{-1}\,s^{-1}$, and the corresponding values for the solute permeability coefficients (B) were 6.11×10^{-7}, 5.69×10^{-7} and 2.22×10^{-7} $m\,s^{-1}$. Other characteristic parameters of the membrane, including structural parameters and tortuosity, were also different for the three cases studied. Song et al. [34] made and optimized a thin-film nanofiber composite PRO (TNC-PRO) flat sheet membrane with a unique support membrane structure. The optimum A and B values were 1.14×10^{-12} $m\,Pa^{-1}\,s^{-1}$ and 4.83×10^{-7} $m\,s^{-1}$, respectively. Another two TNC-PRO flat sheet membranes were made and tested by Bui and McCutcheon [35]. They carried out reverse osmosis (RO) tests to calculate A and B. The values determined for the two coefficients were 1.47×10^{-11} and 7.86×10^{-12} $m\,Pa^{-1}\,s^{-1}$ for A, 1.38×10^{-6} and 1.22×10^{-7} $m\,s^{-1}$ for B. Cui et al. [36] fabricated thin-film composite (TFC) flat sheet membranes consisting of a polyamide thin film layer via interfacial polymerization and a macrovoid-free polyamide support. They obtained A values for three membranes that underwent different treatments of 4.22×10^{-12}, 6.11×10^{-12} and 7.69×10^{-12} $m\,Pa^{-1}\,s^{-1}$. Li et al. [37] fabricated and evaluated TFC polyetherimide (TFC-PEI) flat sheet membranes with three different substrate structures. After using an RO setup, the A values were 4.58×10^{-12}, 5.81×10^{-12} and 6.33×10^{-12} $m\,Pa^{-1}\,s^{-1}$, while the B values were 1.86×10^{-7}, 2.42×10^{-7} and 2.22×10^{-7} $m\,s^{-1}$. In relation to hollow fiber (HF) membranes, inner-selective, outer-selective and double-skinned types have been studied. Chou et al. [38] developed a TFC-PEI HF membrane. A and B were determined in pressure-driven mode, obtaining a value of 4.22×10^{-12} $m\,Pa^{-1}\,s^{-1}$ for A and 6.7×10^{-8} $m\,s^{-1}$ for B. Two outer-selective HF membranes were fabricated and tested by Sun and Chung [39]. For these membranes, A and B were 3.94×10^{-12}, 9.97×10^{-12} $m\,Pa^{-1}\,s^{-1}$ and 1.11×10^{-7}, 5.06×10^{-7} $m\,s^{-1}$, respectively. Han and Chung [40] made four TFC FO membranes to maximize the power density (PD) and minimize the specific reverse salt flux. The A and B values obtained for each membrane after pre-stabilization (30 min) were 1×10^{-11}, 8.61×10^{-12}, 1.19×10^{-11} and 2.5×10^{-11} $m\,Pa^{-1}\,s^{-1}$ for A and 2.03×10^{-7}, 1.69×10^{-7}, 1.31×10^{-7} and 7.14×10^{-6} $m\,s^{-1}$ for B.

For their part, Li ad Chung [41] fabricated and tested four P84-TFC HF membranes, obtaining A values from 2.4×10^{-12} to 2.55×10^{-12} $m\,Pa^{-1}\,s^{-1}$ and B values from 2.08×10^{-8} to 3.83×10^{-8} $m\,s^{-1}$. Fu et al. developed two sandwich-structured outer-selective HF membranes. The B values were not provided numerically in this study but, using the software PlotDigitalizer, were extracted and can be seen in [42]. The values obtained were $A = 4.53 \times 10^{-12}$ and 1.58×10^{-12} $m\,Pa^{-1}\,s^{-1}$, $B = 1.19\times10^{-7}$ and 8.33×10^{-9} $m\,s^{-1}$. Wan and Chung [43] fabricated and tested a TFC-PES (thin film composite-polyethersulfone) HF membrane. This membrane was found to have an A value of 9.72×10^{-12} $m\,Pa^{-1}\,s^{-1}$

and a B value of 1×10^{-7} m s^{-1}. Le et al. [44] fabricated four outer-selective TFC HF membranes. RO tests were performed. Extracted using the WebPlotDigitizer tool, the A and B values for the four membranes were as follows: $A = 8.06 \times 10^{-12}$ m Pa^{-1} s^{-1} and $B = 3.83 \times 10^{-7}$ m s^{-1}, $A = 1.53 \times 10^{-11}$ m Pa^{-1} s^{-1} and $B = 1.47 \times 10^{-6}$ m s^{-1}, $A = 4.50 \times 10^{-12}$ m Pa^{-1} s^{-1} and $B = 2.03 \times 10^{-7}$ m s^{-1}, $A = 6.92 \times 10^{-12}$ m Pa^{-1} s^{-1} and $B = 2.78 \times 10^{-7}$ m s^{-1}. Three outer-selective TFC HF membranes were fabricated by Cheng et al. [45] using three different dopes. The A and B values obtained for the three studied membranes were $A = 4.11 \times 10^{-12}$ m Pa^{-1} s^{-1} and $B = 4.17 \times 10^{-8}$ m s^{-1}, $A = 5.28 \times 10^{-12}$ m Pa^{-1} s^{-1} and $B = 4.44 \times 10^{-8}$ m s^{-1}, $A = 1.47 \times 10^{-12}$ m Pa^{-1} s^{-1} and $B = 1.67 \times 10^{-8}$ m s^{-1}. Han et al. [46] designed a double-skin structure in an HF membrane. The permeability coefficient values obtained were: $A = 4.17 \times 10^{-12}$ m Pa^{-1} s^{-1} and $B = 5.56 \times 10^{-9}$ m s^{-1}. Improving PRO membrane performance by increasing A and/or decreasing B is crucial for the feasibility of the PRO process for electrical energy generation. Quantifying the impact of permeability coefficients on the performance of full-scale PRO system could help to optimize their configuration in terms of the number of membrane modules in series [47,48], the number of stages and the optimal operating points. It should be noted that membrane properties are not the only crucial element in terms of performance in full-scale modules, as fouling [49–51] and spacer designs [33] are also key to estimate the feasibility of the PRO process in long-term operation. Given the lack of extensive experimental work on full-scale PRO systems, simulation tools for predicting the performance of full-scale PRO systems are of fundamental importance [25,52,53]. To carry out appropriate estimations of full-scale PRO systems, certain boundary conditions (with respect to maximum and minimum flows and pressures) should be set by PRO membrane manufacturers and taken into consideration in the simulation process, as happens with full-scale RO systems [54–56].

The aim of this study is to assess the effect of the permeability coefficients A and B on the performance of a single-stage full-scale PRO process. To carry out this study, a simulation tool for full-scale PRO systems was used considering boundary conditions and spiral wound membrane modules (SWMMs). The optimal operating points for $C_{D,in} = 30$ g L^{-1} and $C_{F,in} = 0.5$ g L^{-1} and different ranges of A and B were determined. In this study, only PRO systems in which the energy generating element was a turbine were considered.

2. Material and methods

2.1. Parameters of the PRO SWMMs

There are two commercial PRO SWMMs available (8040 PRO from Toray and HTI OsMem™ 2521). It would be preferable to use the data from the SWMM of Toray given it is an 8-inch module, but there is not enough information in the literature about this module to carry out proper simulations. However, enough data are available for the PRO SWMM HTI OsMem™ 2521. Unfortunately, the latter SWMM is 2.5 inches in diameter and so, for the purposes of this study, was upscaled to an 8 in. diameter using the membrane active surface (S_m) relation between the RO SWMM SW30-2521 and SW30-8040 SWMM (RO process). The S_m values are 1.2 and 37.16 m^2, respectively, for the aforementioned RO SWMMs. The S_m of the OsMem™ 2521 PRO SWMM is 0.5 m^2, and would be 15.53 m^2 for the hypothetical 8 in. diameter OsMem™ PRO SWMM the S_m. As no data are available for the porosity parameters (unit fraction) of the draw (ε_D) and feed (ε_F) sides the values from a published study [57] for RO SWMMs were used. The other PRO SWMM parameters (Table 1) were taken from [58]. Table 1 shows the considered ranges of A and B. The S_m per SWMM is one of the key parameters that affects the performance of PRO systems. In this study, it was considered different values for S_m (from 15.53 to 40.53 m^2) for the best scenario for the PRO system in terms of energy generation (highest A and lowest B).

Table 1
Characteristic parameters of the 8-inch PRO module.

Parameter	Value
A (m Pa^{-1} s^{-1})	2.12×10^{-12}–1.06×10^{-11}
B (m s^{-1})	5.55×10^{-9}–5.55×10^{-7}
S_m (m^2)	15.53
L (m)	1.0
H_D (m)	1.1×10^{-3}
H_F (m)	1.5×10^{-3}
ϵ_D	0.89
ϵ_F	0.65
K (s m^{-1})	3.38×10^{-5}

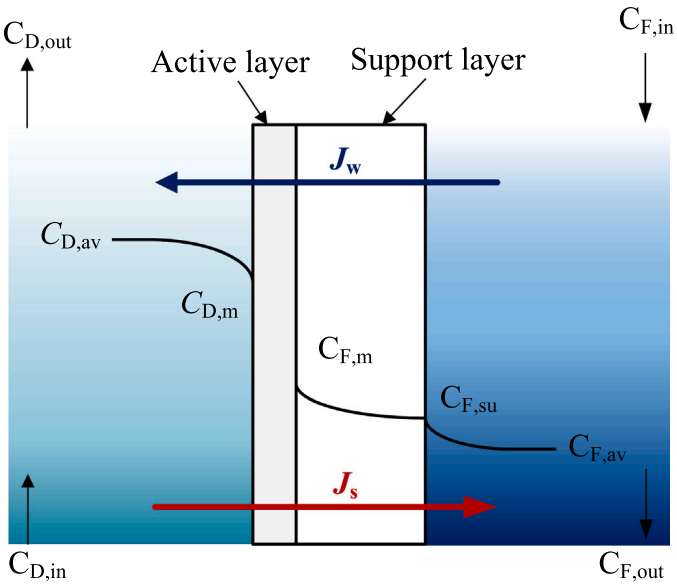

Fig. 1. Concentration profile across the membrane in the PRO process considering both concentration polarizations, ECP and ICP [61].

2.2. Transport equations and simulations

Performance of PRO systems depends on water and solute flux as well as pressures, etc. In the PRO process, transport equations across a semi-permeable membrane that are based on fundamental thermodynamics are used. These fundamentals explain the free energy that is released during the spontaneous mixing of the draw solution (DS) and the feed solution (FS) [59,60]. The equations used for the simulation are listed in Table 2.

It should be noted that to determine $\Delta\pi$, an estimation needs to be made of the membrane surface concentration of both the DS and FS sides. To do so, the effects of external concentration polarization (ECP) and internal concentration polarization (ICP) should be taken into consideration (Fig. 1) [64].

The equations listed in Table 2 were employed in an algorithm simulating full-scale PRO systems which has already been published by the authors [61]. The simulations were carried out considering $C_{D,in} = 30$ g L^{-1}, $C_{F,in} = 0.5$ g L^{-1} of NaCl, $p_{F,in} = 2$ bar and the following ranges: $Q_{D,in}$ and $Q_{F,in}$ from 3 to 16 m^3 h^{-1} in steps of 0.5 m^3 h^{-1} and $p_{D,in}$ from 1 to 20 bar in steps of 0.5 bar.

2.3. Performance assessment

To calculate the amount of energy that can be generated with the full-scale PRO system, it is necessary to know the specific enthalpy (h) in the turbine input and output. Usually, a PRO plant includes devices such as draw and feed pump, an energy recovery device (pressure

Table 2
Transport equations [61].

Permeate flux	$J_p = A(\Delta\pi - \Delta p)$	(1)
Water permeability coefficient	$A = A_0 \cdot TCF \cdot FF$	(2)
Osmotic pressure gradient	$\Delta\pi = \pi_{D,m} - \pi_{F,m}$	(3)
Osmotic pressure	$\pi = 3.805C^2 + 42.527C + 0.434$	(4)
Draw concentration on membrane	$C_{D,m} = \left(C_{D,av} + \frac{J_s}{J_p}\right) e^{\frac{-J_p}{k_D}} - \frac{J_s}{J_p}$	(5)
Feed concentration on membrane	$C_{F,m} = \left(C_{F,av} + \frac{J_s}{J_p}\right) e^{\frac{J_p}{k_F}} e^{KJ_p} - \frac{J_s}{J_p}$	(6)
Average concentration	$C_{x,av} = 0.5(C_{x,in} + C_{x,out})$	(7)
Solute flux	$J_s = J_p \frac{B}{A\beta RT}\left(1 + \frac{A\Delta p}{J_p}\right)$	(8)
Mass transfer coefficient	$k_x = \frac{Sh_x D_{x,av}}{d_{h,x}}$	(9)
Sherwood number in DS [62]	$Sh_D = 1.849\left(Re_D Sc_D \frac{d_{h,D}}{L}\right)^{1/3}(1.002-$	(10)
	$0.0319\gamma_D + 0.00034\gamma_D^2 - 0.001\gamma_D^3)$	(11)
Sherwood number in FS [62]	$Sh_F = 1.849\left(Re_F Sc_F \frac{d_{h,F}}{L}\right)^{1/3}(0.997+$	(12)
	$0.315\gamma_F + 0.022\gamma_F^2 - 0.008\gamma_F^3)$	(13)
Lumped parameter	$\gamma_x = \frac{P_{ew,x}}{\left(Re_x Sc_x \frac{d_{h,x}}{L}\right)^{1/3}}$	(14)
Wall Péclet number	$P_{ew,x} = \frac{J_p d_{h,x}}{D_x}$	(15)
Reynolds number	$Re_x = \frac{\rho_{x,av} \cdot v_{x,av} \cdot d_{h,x}}{\mu_{x,av}}$	(16)
Schmidt number	$Sc_x = \frac{\mu_{x,av}}{\rho_{x,av} \cdot D_x}$	(17)
Solute diffusivity	$D = -1.025 \times 10^{-10}C + 1.518 \times 10^{-9}$	(18)
Density	$\rho = -1.047C^2 + 39.462C + 997.370$	(19)
Dynamic viscosity	$\mu = 0.001\left(0.012C^2 + 0.065C + 0.985\right)$	(20)
Pressure gradient draw side	$\Delta p = p_{D,in} - \frac{PL_D}{2} - p_{F,in} + \frac{PL_F}{2}$	(21)
Pressure losses	$PL_x = \lambda_x \cdot L \cdot \frac{\rho_x}{d_{h,x}} \frac{v_{x,av}^2}{2}$	(22)
Friction factor [63]	$\lambda_x = K_\lambda \cdot 6.23 Re_x^{-0.3}$	(23)
Dilution factor	$DF = \frac{C_{D,out}}{C_{D,in}} = \frac{1 - Y_m}{1}$	(24)
Concentration factor	$CF = \frac{C_{F,out}}{C_{F,in}} = \frac{1}{1 - Y_m}$	(25)
Output concentration of DS	$C_{D,out}(Q_{D,in} + Q_p) = C_{D,in} DF(Q_{D,in} + Q_p) - J_s$	(26)
Output concentration of FS	$C_{F,out}(Q_{F,in} - Q_p) = C_{F,in} CF(Q_{F,in} - Q_p) + J_s$	(27)

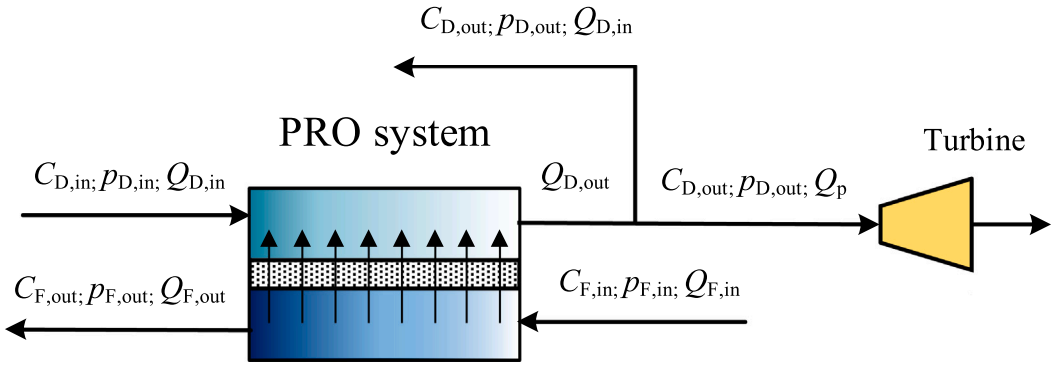

Fig. 2. Flow diagram of the PRO plant.

exchanger and booster pump) and turbine. In this study, only the turbine was considered (Fig. 2) as the energy consumption of the rest of the devices depends on many factors including, for example, the pre-treatment stages. Eqs. (28)–(30) were used to determine h [65]. For non-atmospheric pressures (p_0), specific enthalpy ($h(T, p, C)$) can be estimated using Eq. (30). From the PRO system results, the $P_{TB,\,max}$ and ideal power density (PD_{id}) were calculated using Eqs. (31), (32) and (33) respectively.

$$h(T, p_0, C) = h_w - C(b_1 + b_2 w_s + b_3 w_s^2 + b_4 w_s^3 + b_5 T + b_6 T^2 + b_7 T^3 + b_8 w_s T + b_9 w_s^2 T + b_{10} w_s T^2) \quad (28)$$

$$h_w = 141.355 + 4202.070T - 0.535T^2 + 0.004T^3 \quad (29)$$

$b_1 = -2.348 \times 10^4$, $b_2 = 3.152 \times 10^5$, $b_3 = 2.803 \times 10^6$, $b_4 = -1.446 \times 10^7$, $b_5 = 7.826 \times 10^3$, $b_6 = -4.417 \times 10^1$, $b_7 = 2.139 \times 10^{-1}$, $b_8 = -1.991 \times 10^4$, $b_9 = 2.778 \times 10^4$, $b_{10} = 9.728 \times 10^1$

$$h(T, p, C) = h(T, p_0, C) + \vartheta(p - p_0) \quad (30)$$

where ϑ is the specific volume (the inverse of ρ). ϑ was determined for both the DS and FS solutions using ρ of DS and FS in the input and output of the devices.

$$P_{TB} = \eta_{TB} \dot{m}_{TB} \left(h_{TB,in} - h_{TB,out}\right) \quad (31)$$

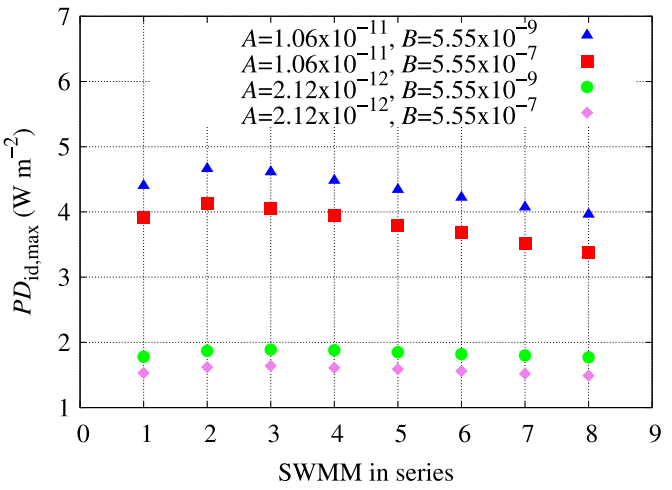

Fig. 3. $PD_{id,max}$ (W m^{-2}) for 1 to 8 SWMMs in series for different values of A and B.

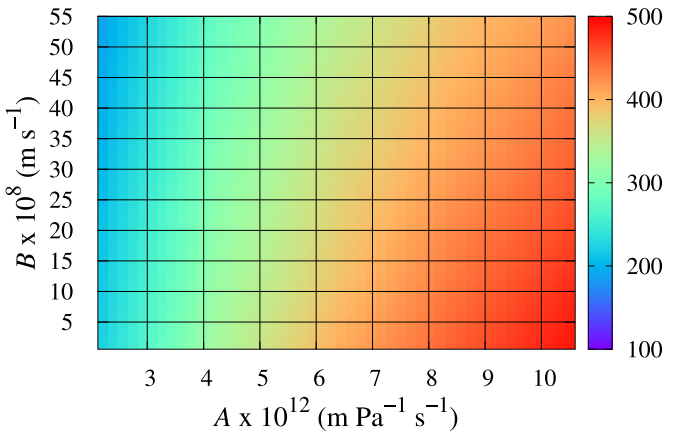

Fig. 4. $P_{TB,\ max}$ (W) for different values of A and B.

$$\dot{m}_{TB} = Q_p \rho_{D,out} \tag{32}$$

$$PD_{id} = \frac{P_{TB}}{nS_m} \tag{33}$$

where η_{TB} is the efficiency of the turbine (assumed as 85%) and n the number of SWMMs in the PRO system.

3. Results and discussion

Fig. 3 shows the maximum power density ($PD_{id,max}$) in a PRO system with 1–8 SWMMs in series. It can be observed that $PD_{id,max}$ was attained with 2 SWMMs in series with $A = 1.06 \times 10^{-11}$ and $B = 5.55 \times 10^{-9}$ and 5.55×10^{-7}. However, $PD_{id,max}$ was attained with 3 SWMMs in series when A was decreased to 2.12×10^{-12}. The difference in terms of $PD_{id,max}$ for 1–8 SWMMs in series was larger for the A decrease than the B increase, even considering that B was increased 100-fold, whereas A was only decreased to 20% of the highest considered value. When B was increased at the highest value of A a difference of about 0.7 W m^{-2} was observed, but the same increase of B at the lowest A value considered showed a difference of about 0.12 W m^{-2}. This means that the Q_p increase had more impact than the solute passage increase. The highest values of $PD_{id,max}$ for the four cases shown in Fig. 3 were 4.66, 4.13, 1.89 and 1.64 W m^{-2}.

The highest values of power in the turbine ($P_{TB,\ max}$) were found with PRO systems with 8 SWMMs in series. Fig. 4 shows $P_{TB,\ max}$ (W) for the ranges considered for A and B (Table 1). As expected, the highest value of $P_{TB,\ max}$ (491.54 W) was obtained for the highest value of A and the lowest value of B. Higher values of A allowed higher Q_p, while lower values of B produced less solute passage allowing higher osmotic pressure differences between the draw and feed sides along the PV. As with $PD_{id,max}$, $P_{TB,\ max}$ was penalized more for decreases in A than for increases in B. For the highest values of both A and B, $P_{TB,\ max}$ was 420.53 W, for the lowest values of A and B it was 220.10 W, while for the lowest value of A and the highest value of B the corresponding value was 185.31 W. That is, a 100-fold increase of B provided a difference in terms of $P_{TB,\ max}$ of 71 W for the highest A and 35 W for the lowest A considered.

Table 3 shows the operating points to obtain $P_{TB,max}$ considering different values of A and B. It can be seen that, for the same value of A, the increase of B decreases $P_{TB,max}$ as well as the values of $p_{D,in}$ and $Q_{D,in}$. The decrease of A results in slight increases of the values of $p_{D,in}$ and $Q_{D,in}$, while the values of $Q_{F,in}$ decrease. In real life operation, a decrease in A may be due to the impact of fouling on the PRO system, as commonly happens in RO systems [29,66]. Fouling can also cause membrane degradation, causing B to increase which would also affect the performance and optimal operating points in PRO systems. The increase of B for different values of A made R change by up to around 3%, which reflects the impact of B on the operating point that maximizes P_{TB}. Taking into consideration $C_{D,in}$ and $C_{F,in}$, the osmotic pressure difference is 2.27 MPa. From Table 3, the increase of $p_{D,in}$ can be seen with the decrease of A and B in the optimal operating points. The ratio between $p_{D,in}$ and the osmotic pressure gradient was in a range of about 0.57–0.66.

Figs. 5 and 6 show the variation of $P_{TB,\ max}$ with the variation of the permeability coefficients A and B. In the case of increases in A, it can be seen that the rise in $P_{TB,\ max}$ is not linear but instead gets smaller as the value of A increases. Fig. 6 shows a more linear relation between B increments and $P_{TB,\ max}$. It should be noted that the increments considered in B are much higher than those considered with A in accordance with the data in the literature. As the impact of A is higher than that of B on $P_{TB,\ max}$, efforts to increase A of new PRO SWMMs should be taken, despite increasing the coefficient B, to make the PRO process viable for energy generation. A 220% increment in terms of $P_{TB,\ max}$ was observed when A was increased 5-fold for 8 SWMMs in series (Fig. 5). This result was quite close to that obtained by Matta et al. [25], however the results obtained in terms of $P_{TB,\ max}$ when B was increased were different from those obtained by Matta et al. [25]. While Matta et al. [25] obtained the same impact in increasing B as A, in this study B was found to have less impact than A. This could be because in the study of Matta et al. [25] a small piece of membrane was considered whereas in our study full-scale PRO SWMMs in series were considered. In addition, the membrane characteristics were different and the pressure drop in DS and FS was not considered by Matta et al. [25]. It should also be mentioned that the relation between $P_{TB,\ max}$ and the increase of A varied depending on the number of SWMMs in series, with the highest being for 1 SWMM and the lowest for 8 SWMMs in series. Another factor that needs to be controlled is the effect of fouling on A as the performance of the PRO system strongly depends on this parameter. It should be noted that fouling can cause the pressure drop to increase, which also affects the performance of these systems, as occurs in RO systems [67].

Tables 4–6 show the operating points to maximize $P_{TB,max}$ considering different values S_m and SWMMs in series. It can be seen that, for the same value of S_m, the increase of SWMMs in series increases $P_{TB,max}$ as well as the values $Q_{F,in}$ for obtaining the maximum $P_{TB,max}$. The operating points to maximize $P_{TB,max}$ change with the SWMMs in series. The higher are the SWMMs in series the lower is $Q_{D,in}$ for getting the highest $P_{TB,max}$ while $p_{D,in}$ varied slightly. The increase of S_m results in slight decreases of the values of $p_{D,in}$ and $Q_{D,in}$, while the

Table 3
Operating points for $P_{TB,max}$ considering one PV with 8 SWMMs in series for different values of A and B ($B_1 = 5.55 \times 10^{-9}$, $B_2 = 3.33 \times 10^{-7}$ $B_3 = 5.55 \times 10^{-7}$)

Parameter	$A = 1.06 \times 10^{-11}$			$A = 6.36 \times 10^{-12}$			$A = 2.12 \times 10^{-12}$		
	B_1	B_2	B_3	B_1	B_2	B_3	B_1	B_2	B_3
$p_{D,in}$ (MPa)	1.45	1.35	1.30	1.50	1.40	1.35	1.50	1.45	1.40
$Q_{D,in}$ (m^3 h^{-1})	14	13.5	13	14.5	14	13.5	15	14.5	14.5
$Q_{F,in}$ (m^3 h^{-1})	6.5	7	7	6	6.5	6.5	5	5.5	5.5
R (%)	28.32	26.86	25.60	24.24	22.11	21.46	15.83	13.38	13.20
$P_{TB,max}$ (W)	491.54	448.42	420.53	403.66	366.80	343.15	220.10	197.56	185.31

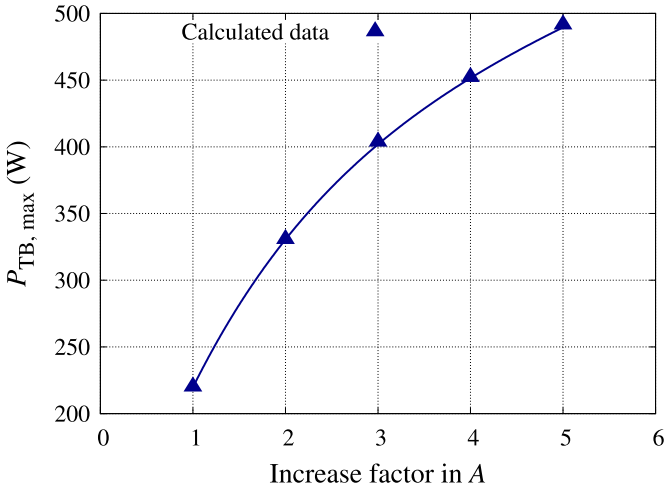

Fig. 5. $P_{TB,\ max}$ (W) variation with increase of A considering 8 SWMMs in series.

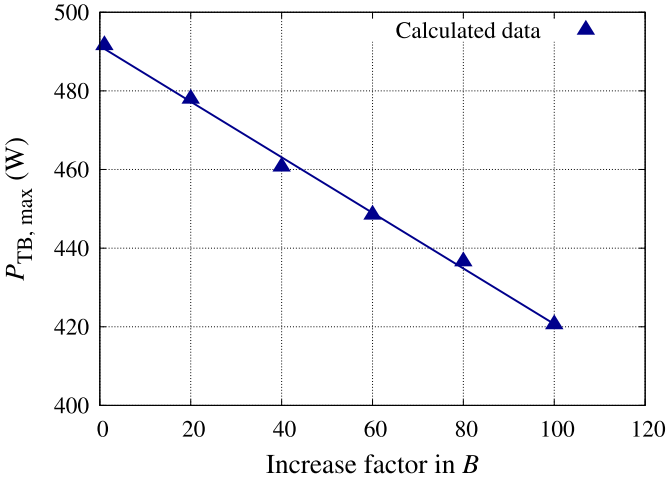

Fig. 6. $P_{TB,\ max}$ (W) variation with increase of B considering 8 SWMMs in series.

values of $Q_{F,in}$ increase. It should be noted that the relation between the increase of S_m and $P_{TB,max}$ is linear. One of the main difficulties when manufacturing PRO SWMMs with high surface density package (m^2/m^3) is the space left for the spacers in both the draw and feed sides. Small spacer height produces a higher pressure drop along the SWMM, causing performance losses. The increase of S_m causes the optimal operating parameters to change (Tables 4–6). It should also be noted that the boundary conditions play an important role in determining the operating points. High values of S_m cause Q_p to increase per SWMM. This in turn causes Q_F to decrease more in comparison with an SWMM of lower S_m. As a result, some operating points that are safe for an SWMM of a particular S_m are not so for other SWMMs with a different S_m. This shows that the characteristic parameters of SWMMs play a

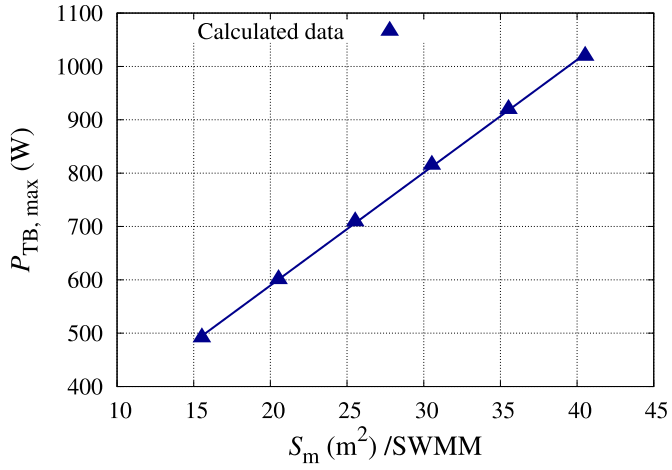

Fig. 7. $P_{TB,\ max}$ (W) variation with increase of S_m/SWMM considering 8 SWMMs in series.

fundamental role in system design and the optimal determination of operating parameters.

Fig. 7 shows the variation of $P_{TB,\ max}$ with the variation of S_m per SWMM considering 1 stage with 8 SWMMs in series. It shows a linear relation between S_m and $P_{TB,\ max}$. A S_m change from 20.53 to 40.53 m^2/SWMM produced an increment of 418.54 W in terms of $P_{TB,\ max}$. By increasing S_m, parameters such as H_D and H_F may be forced to change producing different velocity profiles along SWMMs and different performance estimation. These variations were not considered in this study. It should be noted that the actual PRO SWMMs does not have such packing density (m^2/m^3), efforts to increase S_m of new PRO SWMMs should be taken to make the PRO process viable for energy generation.

4. Conclusions

In this simulation-based study, the impact of variation of the water and solute permeability coefficients, A and B, was evaluated. The results indicate that variation of A has a higher impact on the performance of full-scale PRO systems with SWMMs than B. According to these results, PRO membrane manufacturers should focus, among other things, on increasing A even if this entails an increase in B. The maximum amount of energy that could be generated considering a single-stage system with one pressure vessel and 8 SWMMs in series was about 500 W. It should be noted that in PRO plants it is usually not possible to measure all the parameters needed to carry out precise simulations, so there will be variability and uncertainties in performance estimations. The actual amount of energy that would be generated will depend on the efficiency of the devices and the pre-treatment required for both the draw and feed solutions. The results obtained may be useful for estimating the impact of fouling in PRO systems, as one of the main consequences of fouling is a decrease in A with operating time. In order to increase the amount of energy that can be generated with PRO systems, the membrane area per element should also be increased. The

Table 4
Operating points for highest $P_{TB,max}$ with $S_m = 20.53$ m^2/SWMM.

	SWMMs in series							
Parameter	1	2	3	4	5	6	7	8
$p_{D,in}$ (MPa)	1.30	1.30	1.35	1.30	1.40	1.30	1.40	1.30
$Q_{D,in}$ (m^3 h^{-1})	15.5	15	15	14.5	14.5	14	14	13.5
$Q_{F,in}$ (m^3 h^{-1})	6	6	6.5	7	7	8	8	8.5
R (%)	5.80	11.67	15.16	18.84	20.87	23.10	23.84	27.15
$P_{TB,max}$ (W)	90.33	182.43	266.89	342.97	413.28	480.40	540.23	600.74

Table 5
Operating points for highest $P_{TB,max}$ with $S_m = 30.53$ m^2/SWMM.

	SWMMs in series							
Parameter	1	2	3	4	5	6	7	8
$p_{D,in}$ (MPa)	1.25	1.20	1.20	1.20	1.20	1.25	1.15	1.15
$Q_{D,in}$ (m^3 h^{-1})	15.5	15	14.5	14	13.5	13.5	13	12.5
$Q_{F,in}$ (m^3 h^{-1})	8	8.5	9	10	10.5	11	12	12.5
R (%)	6.03	11.52	15.65	18.01	20.59	21.87	24.83	26.30
$P_{TB,max}$ (W)	130.72	253.72	365.34	467.61	562.13	652.18	737.30	815.00

Table 6
Operating points for highest $P_{TB,max}$ with $S_m = 40.53$ m^2/SWMM.

	SWMMs in series							
Parameter	1	2	3	4	5	6	7	8
$p_{D,in}$ (MPa)	1.15	1.15	1.15	1.15	1.15	1.10	1.20	1.20
$Q_{D,in}$ (m^3 h^{-1})	15	14.5	14	13.5	13	12.5	12.5	12
$Q_{F,in}$ (m^3 h^{-1})	11	10.5	12	13	13.5	14.5	15	15.5
R (%)	5.91	11.82	14.84	17.54	20.31	22.96	22.89	24.47
$P_{TB,max}$ (W)	167.06	318.94	457.68	585.81	704.71	815.95	921.94	1019.28

increase in membrane area per element causes the optimal operating points to change even if the element has the same A and B. The optimal operating points vary with the permeability coefficients, making it crucial to develop a control design system that allows optimization of the operation of PRO systems. Considering more than one stage would also increase the amount of energy that could be generated. The increase in membrane area per element may result in changes to the optimal design of PRO systems as the safe operating windows are also affected. Further studies should be carried out using experimental data of full-scale PRO system working with real operating conditions to improve the modeling, simulation, optimization and fouling effect on full-scale PRO systems.

Declaration of competing interest

The authors declare that they have no known competing financial interests or personal relationships that could have appeared to influence the work reported in this paper.

Data availability

No data was used for the research described in the article.

Acknowledgments

This research was co-funded by the European Regional Development Fund (ERDF) and the ACLIEMAC Project (MAC2/3.5b/380) of the INTERREG V-A MAC 2014–2020 program. F. Tadeo was partially funded through MCIN/AEI/10.13039/501100011033, and NextGenerationEU/PRTR TED2021-129716B-I00.

References

[1] M.A. Bagherian, K. Mehranzamir, A comprehensive review on renewable energy integration for combined heat and power production, Energy Convers. Manag. 224 (2020) 113454, http://dx.doi.org/10.1016/j.enconman.2020.113454.

[2] R.H. Moss, J.A. Edmonds, K.A. Hibbard, M.R. Manning, S.K. Rose, D.P. Van Vuuren, T.R. Carter, S. Emori, M. Kainuma, T. Kram, et al., The next generation of scenarios for climate change research and assessment, Nature 463 (7282) (2010) 747–756.

[3] P. Makolo, R. Zamora, T.-T. Lie, The role of inertia for grid flexibility under high penetration of variable renewables - a review of challenges and solutions, Renew. Sust. Energ. Rev. 147 (2021) 111223, http://dx.doi.org/10.1016/j.rser.2021.111223.

[4] Z. Zhang, T. Ding, Q. Zhou, Y. Sun, M. Qu, Z. Zeng, Y. Ju, L. Li, K. Wang, F. Chi, A review of technologies and applications on versatile energy storage systems, Renew. Sust. Energ. Rev. 148 (2021) 111263, http://dx.doi.org/10.1016/j.rser.2021.111263.

[5] Z.M. Binger, G. O'Toole, A. Achilli, Evidence of solution-diffusion-with-defects in an engineering-scale pressure retarded osmosis system, J. Membr. Sci. 625 (2021) 119135, http://dx.doi.org/10.1016/j.memsci.2021.119135.

[6] U. Safder, J.Y. Lim, B.S. How, P. Ifaei, S. Heo, C. Yoo, Optimal configuration and economic analysis of PRO-retrofitted industrial networks for sustainable energy production and material recovery considering uncertainties: Bioethanol and sugar mill case study, Renew. Energy 182 (2022) 797–816, http://dx.doi.org/10.1016/j.renene.2021.10.047.

[7] R.R. Gonzales, A. Abdel-Wahab, S. Adham, D.S. Han, S. Phuntsho, W. Suwaileh, N. Hilal, H.K. Shon, Salinity gradient energy generation by pressure retarded osmosis: A review, Desalination 500 (2021) 114841, http://dx.doi.org/10.1016/j.desal.2020.114841.

[8] M. Tawalbeh, A. Al-Othman, N. Abdelwahab, A.H. Alami, A.G. Olabi, Recent developments in pressure retarded osmosis for desalination and power generation, Renew. Sust. Energ. Rev. 138 (2021) 110492, http://dx.doi.org/10.1016/j.rser.2020.110492.

[9] N.J. Kaleekkal, J. Nambikkattu, A. Rasheeda Satheesh, R.R. Gonzales, H.K. Shon, S. Vigneswaran, Engineered osmosis – sustainable technology for water recovery, product concentration and energy generation, Environ. Sci.: Water Res. Technol. 8 (2022) 1326–1358, http://dx.doi.org/10.1039/D2EW00005A.

[10] C. Seyfried, H. Palko, L. Dubbs, Potential local environmental impacts of salinity gradient energy: A review, Renew. Sust. Energ. Rev. 102 (2019) 111–120, http://dx.doi.org/10.1016/j.rser.2018.12.003.

[11] N. Bajraktari, C. Hélix-Nielsen, H.T. Madsen, Pressure retarded osmosis from hypersaline sources — A review, Desalination 413 (2017) 65–85, http://dx.doi.org/10.1016/j.desal.2017.02.017.

[12] T.T.D. Tran, K. Park, A.D. Smith, System scaling approach and thermoeconomic analysis of a pressure retarded osmosis system for power production with hypersaline draw solution: A Great Salt Lake case study, Energy 126 (2017) 97–111, http://dx.doi.org/10.1016/j.energy.2017.03.002.

[13] Y. Jiao, L. Song, C. Zhao, Y. An, W. Lu, B. He, C. Yang, Membrane-based indirect power generation technologies for harvesting salinity gradient energy

- a review, Desalination 525 (2022) 115485, http://dx.doi.org/10.1016/j.desal.2021.115485.
[14] A.P. Straub, A. Deshmukh, M. Elimelech, Pressure-retarded osmosis for power generation from salinity gradients: Is it viable? Energy Environ. Sci. 9 (2016) 31–48, http://dx.doi.org/10.1039/C5EE02985F.
[15] X. Zhou, W.-B. Zhang, J.-J. Li, X. Bao, X.-W. Han, M. Myintzu Theint, X.-J. Ma, An electrochemical system for salinity gradient energy harvesting, Energy Convers. Manag. 255 (2022) 115315, http://dx.doi.org/10.1016/j.enconman.2022.115315.
[16] G. Han, J.T. Liu, K.J. Lu, T.-S. Chung, Advanced anti-fouling membranes for osmotic power generation from wastewater via pressure retarded osmosis (PRO), Environ. Sci. Technol. 52 (11) (2018) 6686–6694, http://dx.doi.org/10.1021/acs.est.7b05933, PMID: 29741369.
[17] S. Liu, W. Song, M. Meng, M. Xie, Q. She, P. Zhao, X. Wang, Engineering pressure retarded osmosis membrane bioreactor (PRO-MBR) for simultaneous water and energy recovery from municipal wastewater, Sci. Total Environ. 826 (2022) 154048, http://dx.doi.org/10.1016/j.scitotenv.2022.154048.
[18] W.Y. Chia, S.R. Chia, K.S. Khoo, K.W. Chew, P.L. Show, Sustainable membrane technology for resource recovery from wastewater: Forward osmosis and pressure retarded osmosis, J. Water Process. Eng. 39 (2021) 101758, http://dx.doi.org/10.1016/j.jwpe.2020.101758.
[19] N.Y. Yip, M. Elimelech, Comparison of energy efficiency and power density in pressure retarded osmosis and reverse electrodialysis, Environ. Sci. Technol. 48 (18) (2014) 11002–11012, http://dx.doi.org/10.1021/es5029316, PMID: 25157687.
[20] C. Lee, S.H. Chae, E. Yang, S. Kim, J.H. Kim, I.S. Kim, A comprehensive review of the feasibility of pressure retarded osmosis: Recent technological advances and industrial efforts towards commercialization, Desalination 491 (2020) 114501, http://dx.doi.org/10.1016/j.desal.2020.114501.
[21] M. Kishimoto, Y. Tanaka, M. Yasukawa, S. Goda, M. Higa, H. Matsuyama, Optimization of pressure-retarded osmosis with hollow-fiber membrane modules by numerical simulation, Ind. Eng. Chem. Res. 58 (16) (2019) 6687–6695, http://dx.doi.org/10.1021/acs.iecr.9b00139.
[22] K. Touati, F. Tadeo, Study of the reverse salt diffusion in pressure retarded osmosis: Influence on concentration polarization and effect of the operating conditions, Desalination 389 (2016) 171–186, http://dx.doi.org/10.1016/j.desal.2016.02.014, Pressure Retarded Osmosis.URL https://www.sciencedirect.com/science/article/pii/S0011916416300522.
[23] A.P. Straub, S. Lin, M. Elimelech, Module-scale analysis of pressure retarded osmosis: Performance limitations and implications for full-scale operation, Environ. Sci. Technol. 48 (20) (2014) 12435–12444, http://dx.doi.org/10.1021/es503790k, PMID: 25222561.
[24] N. AlZainati, H. Saleem, A. Altaee, S.J. Zaidi, M. Mohsen, A. Hawari, G.J. Millar, Pressure retarded osmosis: Advancement, challenges and potential, J. Water Process. Eng. 40 (2021) 101950, http://dx.doi.org/10.1016/j.jwpe.2021.101950.
[25] S.M. Matta, M.A. Selam, H. Manzoor, S. Adham, H.K. Shon, M. Castier, A. Abdel-Wahab, Predicting the performance of spiral-wound membranes in pressure-retarded osmosis processes, Renew. Energy 189 (2022) 66–77, http://dx.doi.org/10.1016/j.renene.2022.02.125.
[26] Y. Tanaka, M. Yasukawa, S. Goda, H. Sakurai, M. Shibuya, T. Takahashi, M. Kishimoto, M. Higa, H. Matsuyama, Experimental and simulation studies of two types of 5-inch scale hollow fiber membrane modules for pressure-retarded osmosis, Desalination 447 (2018) 133–146, http://dx.doi.org/10.1016/j.desal.2018.09.015.
[27] J. Benjamin, S. AL Mashrafi, A. Tejada-Martinez, N. Diaz-Elsayed, M.E. Arias, Q. Zhang, Optimizing pressure retarded osmosis spacer geometries: An experimental and CFD modeling study, J. Membr. Sci. 647 (2022) 120284, http://dx.doi.org/10.1016/j.memsci.2022.120284.
[28] N.A. Pham, D.Y.F. Ng, K. Goh, Z. Dong, R. Wang, Assessing the potential of integrally skinned asymmetric hollow fiber membranes for addressing membrane fouling in pressure retarded osmosis process, Desalination 520 (2021) 115347, http://dx.doi.org/10.1016/j.desal.2021.115347.
[29] J. Ju, Y. Choi, S. Lee, N. Jeong, Comparison of fouling characteristics between reverse electrodialysis (RED) and pressure retarded osmosis (PRO), Desalination 497 (2021) 114648, http://dx.doi.org/10.1016/j.desal.2020.114648.
[30] J. Fei, Y. Lyu, X. Zhong, D.E. Wiley, Z. Liu, Q. She, Calcium phosphate scaling in osmotically driven membrane processes: Limiting flux behavior and its implications for scaling mitigation, J. Membr. Sci. 631 (2021) 119351, http://dx.doi.org/10.1016/j.memsci.2021.119351.
[31] S.J. Kwon, K. Park, D.Y. Kim, M. Zhan, S. Hong, J.-H. Lee, High-performance and durable pressure retarded osmosis membranes fabricated using hydrophilized polyethylene separators, J. Membr. Sci. 619 (2021) 118796, http://dx.doi.org/10.1016/j.memsci.2020.118796.
[32] Y.S. Khoo, W.J. Lau, H. Chamani, T. Matsuura, A.F. Ismail, Water flux increase by inverting the membrane from its normal position – is it occurring in FO and PRO? J. Water Process. Eng. 37 (2020) 101366, http://dx.doi.org/10.1016/j.jwpe.2020.101366.
[33] Q. She, D. Hou, J. Liu, K.H. Tan, C.Y. Tang, Effect of feed spacer induced membrane deformation on the performance of pressure retarded osmosis (PRO): Implications for PRO process operation, J. Membr. Sci. 445 (2013) 170–182, http://dx.doi.org/10.1016/j.memsci.2013.05.061.
[34] X. Song, Z. Liu, D.D. Sun, Energy recovery from concentrated seawater brine by thin-film nanofiber composite pressure retarded osmosis membranes with high power density, Energy Environ. Sci. 6 (4) (2013) 1199–1210.
[35] N.-N. Bui, J.R. McCutcheon, Nanofiber supported thin-film composite membrane for pressure-retarded osmosis, Environ. Sci. Technol. 48 (7) (2014) 4129–4136, http://dx.doi.org/10.1021/es4037012, PMID: 24387600.
[36] Y. Cui, X.-Y. Liu, T.-S. Chung, Enhanced osmotic energy generation from salinity gradients by modifying thin film composite membranes, Chem. Eng. J. 242 (2014) 195–203, http://dx.doi.org/10.1016/j.cej.2013.12.078.
[37] Y. Li, R. Wang, S. Qi, C. Tang, Structural stability and mass transfer properties of pressure retarded osmosis (PRO) membrane under high operating pressures, J. Membr. Sci. 488 (2015) 143–153, http://dx.doi.org/10.1016/j.memsci.2015.04.030.
[38] S. Chou, R. Wang, A.G. Fane, Robust and high performance hollow fiber membranes for energy harvesting from salinity gradients by pressure retarded osmosis, J. Membr. Sci. 448 (2013) 44–54, http://dx.doi.org/10.1016/j.memsci.2013.07.063.
[39] S.-P. Sun, T.-S. Chung, Outer-selective pressure-retarded osmosis hollow fiber membranes from vacuum-assisted interfacial polymerization for osmotic power generation, Environ. Sci. Technol. 47 (22) (2013) 13167–13174, http://dx.doi.org/10.1021/es403270n, PMID: 24117418.
[40] G. Han, T.-S. Chung, Robust and high performance pressure retarded osmosis hollow fiber membranes for osmotic power generation, AIChE J. 60 (3) (2014) 1107–1119, http://dx.doi.org/10.1002/aic.14342, arXiv:https://aiche.onlinelibrary.wiley.com/doi/pdf/10.1002/aic.14342.
[41] X. Li, T.-S. Chung, Thin-film composite P84 co-polyimide hollow fiber membranes for osmotic power generation, Appl. Energy 114 (2014) 600–610, http://dx.doi.org/10.1016/j.apenergy.2013.10.037.
[42] T.-s. Chung, C.F. Wan, Membrane Technology for Osmotic Power Generation By Pressure Retarded Osmosis, CRC Press, 2020.
[43] C.F. Wan, T.-S. Chung, Osmotic power generation by pressure retarded osmosis using seawater brine as the draw solution and wastewater retentate as the feed, J. Membr. Sci. 479 (2015) 148–158, http://dx.doi.org/10.1016/j.memsci.2014.12.036.
[44] N.L. Le, N.M.S. Bettahalli, S.P. Nunes, T.-S. Chung, Outer-selective thin film composite (TFC) hollow fiber membranes for osmotic power generation, J. Membr. Sci. 505 (2016) 157–166, http://dx.doi.org/10.1016/j.memsci.2016.01.027.
[45] Z.L. Cheng, X. Li, Y. Feng, C.F. Wan, T.-S. Chung, Tuning water content in polymer dopes to boost the performance of outer-selective thin-film composite (TFC) hollow fiber membranes for osmotic power generation, J. Membr. Sci. 524 (2017) 97–107, http://dx.doi.org/10.1016/j.memsci.2016.11.009.
[46] G. Han, Z.L. Cheng, T.-S. Chung, Thin-film composite (TFC) hollow fiber membrane with double-polyamide active layers for internal concentration polarization and fouling mitigation in osmotic processes, J. Membr. Sci. 523 (2017) 497–504, http://dx.doi.org/10.1016/j.memsci.2016.10.022.
[47] S. Sarp, N. Hilal, Thermodynamic optimization of multistage pressure retarded osmosis (MPRO) with variable feed pressures for hypersaline solutions, Desalination 477 (2020) 114245, http://dx.doi.org/10.1016/j.desal.2019.114245.
[48] H.W. Chung, J. Swaminathan, J.H. Lienhard, Multistage pressure-retarded osmosis configurations: A unifying framework and thermodynamic analysis, Desalination 476 (2020) 114230, http://dx.doi.org/10.1016/j.desal.2019.114230.
[49] M. Zhang, D. Hou, Q. She, C.Y. Tang, Gypsum scaling in pressure retarded osmosis: Experiments, mechanisms and implications, Water Res. 48 (2014) 387–395, http://dx.doi.org/10.1016/j.watres.2013.09.051.
[50] P.-F. Sun, Y. Jang, S.-Y. Ham, H. Ryoo, H.-D. Park, Effects of reverse solute diffusion on membrane biofouling in pressure-retarded osmosis processes, Desalination 512 (2021) 115145, http://dx.doi.org/10.1016/j.desal.2021.115145.
[51] J. Fei, W. Mai, P.S. Cheng, J. Shi, Z. Liu, Q. She, Membrane structure-dependent limiting flux behavior and membrane selectivity loss during gypsum scaling: Implications for pressure-retarded osmosis operation and membrane design, Desalination 492 (2020) 114644, http://dx.doi.org/10.1016/j.desal.2020.114644.
[52] H. Manzoor, M.A. Selam, F.B. Abdur Rahman, S. Adham, M. Castier, A. Abdel-Wahab, A tool for assessing the scalability of pressure-retarded osmosis (PRO) membranes, Renew. Energy 149 (2020) 987–999, http://dx.doi.org/10.1016/j.renene.2019.10.098.
[53] H. Manzoor, M.A. Selam, S. Adham, H.K. Shon, M. Castier, A. Abdel-Wahab, Energy recovery modeling of pressure-retarded osmosis systems with membrane modules compatible with high salinity draw streams, Desalination 493 (2020) 114624, http://dx.doi.org/10.1016/j.desal.2020.114624.
[54] A. Ruiz-García, I. Nuez, Simulation-based assessment of safe operating windows and optimization in full-scale seawater reverse osmosis systems, Desalination 533 (2022) 115768, http://dx.doi.org/10.1016/j.desal.2022.115768.
[55] A. Ruiz-García, I. de la Nuez-Pestana, A computational tool for designing BWRO systems with spiral wound modules, Desalination 426 (2018) 69–77, http://dx.doi.org/10.1016/j.desal.2017.10.040.

[56] A. Ruiz-García, I. Nuez, Performance evaluation and boron rejection in a SWRO system under variable operating conditions, Comput. Chem. Eng. 153 (2021) 107441, http://dx.doi.org/10.1016/j.compchemeng.2021.107441.

[57] G. Schock, A. Miquel, Mass transfer and pressure loss in spiral wound modules, Desalination 64 (1987) 339–352, http://dx.doi.org/10.1016/0011-9164(87)90107-X.

[58] D. Attarde, M. Jain, K. Chaudhary, S.K. Gupta, Osmotically driven membrane processes by using a spiral wound module — Modeling, experimentation and numerical parameter estimation, Desalination 361 (2015) 81–94, http://dx.doi.org/10.1016/j.desal.2015.01.025.

[59] N.Y. Yip, A. Tiraferri, W.A. Phillip, J.D. Schiffman, L.A. Hoover, Y.C. Kim, M. Elimelech, Thin-film composite pressure retarded osmosis membranes for sustainable power generation from salinity gradients, Environ. Sci. Technol. 45 (10) (2011) 4360–4369, http://dx.doi.org/10.1021/es104325z, PMID: 21491936.

[60] S. Loeb, Production of energy from concentrated brines by pressure-retarded osmosis: I. Preliminary technical and economic correlations, J. Membr. Sci. 1 (1976) 49–63, http://dx.doi.org/10.1016/S0376-7388(00)82257-7.

[61] A. Ruiz-García, F. Tadeo, I. Nuez, Simulation tool for full-scale PRO systems using SWMMs, Desalination 541 (2022) 116025, http://dx.doi.org/10.1016/j.desal.2022.116025.

[62] C.H. Tan, H.Y. Ng, Revised external and internal concentration polarization models to improve flux prediction in forward osmosis process, Desalination 309 (2013) 125–140, http://dx.doi.org/10.1016/j.desal.2012.09.022.

[63] V. Geraldes, N.E. Pereira, M.N. de Pinho, Simulation and optimization of medium-sized seawater reverse osmosis processes with spiral-wound modules, Ind. Eng. Chem. Res. 44 (6) (2005) 1897–1905, http://dx.doi.org/10.1021/ie049357s.

[64] K. Touati, C. Hänel, F. Tadeo, T. Schiestel, Effect of the feed and draw solution temperatures on PRO performance: Theoretical and experimental study, Desalination 365 (2015) 182–195, http://dx.doi.org/10.1016/j.desal.2015.02.016.

[65] M.H. Sharqawy, J.H. Lienhard V., S.M. Zubair, On exergy calculations of seawater with applications in desalination systems, Int. J. Therm. Sci. 50 (2) (2011) 187–196, http://dx.doi.org/10.1016/j.ijthermalsci.2010.09.013.

[66] N. Najid, J.N. Hakizimana, S. Kouzbour, B. Gourich, A. Ruiz-García, C. Vial, Y. Stiriba, R. Semiat, Fouling control and modeling in reverse osmosis for seawater desalination: A review, Comput. Chem. Eng. 162 (2022) 107794, http://dx.doi.org/10.1016/j.compchemeng.2022.107794.

[67] A. Ruiz-García, I. Nuez, A time-dependent model of pressure drop in reverse osmosis spiral wound membrane modules, IFAC-PapersOnLine 54 (3) (2021) 158–163, http://dx.doi.org/10.1016/j.ifacol.2021.08.235, 16th IFAC Symposium on Advanced Control of Chemical Processes ADCHEM 2021.